19

Dissipative Structures

19.1 The Constructive Role of Irreversible Processes

One of the most profound lessons of nonequilibrium thermodynamics is the dual role of irreversible processes: as destroyers of order near equilibrium and as creators of order far from equilibrium. For far-from-equilibrium systems, there are no general extremum principles that predict the state to which it will evolve. The lack of extremum principles that uniquely predict the state to which a nonequilibrium system will evolve is a fundamental aspect of nonequilibrium systems. In stark contrast to equilibrium systems, which evolve to a state that minimizes a free energy, nonequilibrium systems can evolve unpredictably; their state cannot always be uniquely specified by macroscopic rate equations. This is because, for a given set of nonequilibrium conditions, it is often possible to have more than one state. As a result of random fluctuations, or other random factors such as small inhomogeneities or imperfections, the system evolves to one of the many possible states. Which one of these states a particular system will evolve to is, in general, not predictable. The new states thus attained are often 'ordered states' that possess spatiotemporal organization. Patterns in fluid flow, inhomogeneities in concentrations exhibiting geometrical patterns with great symmetry or periodic variations of concentrations are examples of such ordered states. Because of its fundamental character, we shall refer to the general phenomenon of a nonequilibrium system evolving to an ordered state as a result of fluctuations as **order through fluctuations** [1, 2].

In nonequilibrium systems, oscillating concentrations and geometrical concentration patterns can be a result of chemical reactions and diffusion, the same dissipative processes that, in an isolated system, wipe out inhomogeneities and drive the system to a stationary, timeless homogeneous state of equilibrium. Since the creation and maintenance of organized nonequilibrium structures are due to dissipative processes, they are called **dissipative structures** [3].

The two concepts of *dissipative structures* and *order through fluctuations* encapsulate the main aspects of nonequilibrium order that we describe in this chapter.

19.2 Loss of Stability, Bifurcation and Symmetry Breaking

In the previous chapter we have seen that the stability of the thermodynamic branch is no longer assured when a system is driven far from equilibrium. In Section 18.3 we have seen how a necessary condition (18.3.7) for

Modern Thermodynamics: From Heat Engines to Dissipative Structures, Second Edition. Dilip Kondepudi and Ilya Prigogine.

a system to become unstable can be obtained by using the second variation of entropy, $\delta^2 S$. Beyond this point, we are confronted with a multiplicity of states and unpredictability. To understand the precise conditions for instability and the subsequent behavior of a system, we need to use the specific features of the system, such as the rates of chemical reactions and the hydrodynamic equations. There are, however, some general features of far-from-equilibrium systems that we will summarize in this section. A detailed discussion of dissipative structures will be presented in the following sections.

The loss of stability of a nonequilibrium state can be analyzed using the general theory of stability for solutions of a nonlinear differential equation. Here we encounter the basic relationship between the loss of stability, multiplicity of solutions and symmetry. We also encounter the phenomenon of 'bifurcation' or 'branching' of new solutions of a differential equation from a particular solution. We shall first illustrate these general features for a simple nonlinear differential equation and then show how they are used to describe far-from-equilibrium systems.

19.2.1 An Elementary Example of Bifurcation and Symmetry Breaking

Consider the equation

$$\frac{d\alpha}{dt} = -\alpha^3 + \lambda\alpha \tag{19.2.1}$$

in which λ is a parameter. Our objective is to study the stationary solutions of this equation as a function of λ. Equation (19.2.1) possesses a simple twofold symmetry: it remains invariant when α is replaced by $-\alpha$. This means that if $\alpha(t)$ is a solution, then $-\alpha(t)$ is also a solution. If $\alpha(t) \neq -\alpha(t)$, then there are two solutions to the equation. In this way, symmetry and multiplicity of solutions are related.

The stationary states of this differential equation are

$$\alpha = 0, \quad \alpha = \pm\sqrt{\lambda} \tag{19.2.2}$$

Note the multiplicity of solutions related to symmetry. When a solution does not possess the symmetries of the differential equation, i.e. when $\alpha \neq -\alpha$, it is said to be a solution with a **broken symmetry** or a solution that has broken the symmetry. In this case, the solution $\alpha = 0$ is invariant when α is replaced by $-\alpha$, but the solution $\alpha = \pm\sqrt{\lambda}$ is not. Hence $\alpha = \pm\sqrt{\lambda}$ is said to have broken the symmetry of the differential equation. (Though this idea may seem rather trivial in this simple case, it has a rather important and nontrivial significance for nonequilibrium systems.)

Let us assume that, for physical reasons, we are seeking only real solutions of Equation (19.2.1). When $\lambda < 0$ there is only one real solution, but when $\lambda > 0$ there are three solutions, as shown in Figure 19.1. The new solutions for $\lambda > 0$ *branch* or *bifurcate* from the solution $\alpha = 0$. The value of λ at which new solutions bifurcate

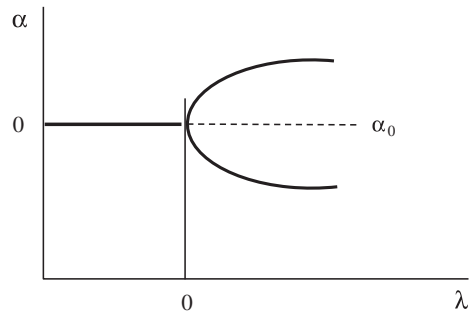

Figure 19.1 *The bifurcation of solutions $\alpha = 0$ and $\alpha = \pm\sqrt{\lambda}$ to Equation (19.2.1) as a function of the parameter λ. The dashed line represents an unstable solution.*

is called the **bifurcation point**. In Figure 19.1, $\lambda = 0$ is the bifurcation point. A similar bifurcation of new solutions from a given solution occurs generally in nonlinear equations, be they a simple algebraic equation as above, a set of coupled ordinary differential equations or more complex partial differential equations.

Turning to the question of stability, we shall now see that the solution $\alpha = 0$ becomes unstable precisely at the point where new solutions $\alpha = \pm\sqrt{\lambda}$ emerge. As we have seen earlier, a stationary solution α_s is locally stable if a small perturbation $\delta(t)$ from the solution decays to the stationary state. Thus we must look at the time evolution of $\alpha = \alpha_s + \delta(t)$ to determine if α_s is stable or not. Substituting $\alpha = \alpha_s + \delta(t)$ into Equation (19.2.1), and keeping only terms of the first order in δ, we obtain

$$\frac{d\delta}{dt} = -3\alpha_s^2\delta + \lambda\delta \tag{19.2.3}$$

For the stationary state $\alpha_s = 0$, we see that the solution is stable if $\lambda < 0$, because $\delta(t)$ decays exponentially. On the other hand, if $\lambda > 0$ the solution is locally unstable because $\delta(t)$ grows exponentially. At the same time, if we use Equation (19.2.3) to analyze the stability of the stationary states $\alpha_s = \pm\sqrt{\lambda}$, we find that they are stable. These stability properties of the stationary states mean that, as λ moves from a value less than zero to a value greater than zero, the solution $\alpha = 0$ becomes unstable and the system makes a transition to one of the two new solutions that bifurcate at $\lambda = 0$. To which of the two possible states the system will evolve is not deterministic; it depends on the random fluctuations in the system. The loss of stability implies that a random fluctuation will grow and drive the system to one of the two states, $\alpha_s = +\sqrt{\lambda}$ or $\alpha_s = -\sqrt{\lambda}$.

The bifurcation of new solutions at exactly the point where one solution loses stability is not a coincidence, it is a general property of the solutions of nonlinear equations. (This general relation between bifurcation and stability of solutions of nonlinear equations can be explained using *topological degree theory*, which is beyond the scope of this discussion.)

19.2.2 General Theory of Bifurcation

In far-from-equilibrium systems the loss of stability of the thermodynamic branch and the transition to a dissipative structure follows the same general features shown in the above simple example. The parameter such as λ corresponds to constraints – e.g. flow rates or concentrations maintained at a nonequilibrium value – that keep the system away from equilibrium. When λ reaches a particular value, the thermodynamic branch becomes unstable but at the same time new solutions now become possible; driven by fluctuations, the system makes a transition to one of the new states. As we did in Section 18.4, let us specify the state of the system by $X_k,\ k = 1,\ 2, \ldots, n$ which, in general, may be functions of both position $\mathbf{r}$ and time t. Let the equation that describes the spatiotemporal evolution of the system be

$$\frac{\partial X_k}{\partial t} = Z_k\left(X_i, \lambda\right) \tag{19.2.4}$$

Here λ is the nonequilibrium constraint. If the system under consideration is a homogeneous chemical system, then Z_k is specified by the rates of chemical reactions. For an inhomogeneous system, Z_k may contain partial derivatives to account for diffusion and other transport processes. It is remarkable that, whatever the complexity of Z_k, the loss of stability of a solution of Equation (19.2.4) at a particular value of λ and bifurcation of new solutions at this point are similar to those of Equation (19.2.1). As in the case of Equation (19.2.1), the symmetries of Equation (19.2.4) are related to the multiplicity of solutions. For example, in an isotropic system, the equations should be invariant under the inversion $\mathbf{r} \to -\mathbf{r}$. In this case, if $X_k(\mathbf{r}, t)$ is a solution then $X_k(-\mathbf{r}, t)$ will also be a solution; if $X_k(\mathbf{r}, t) \neq X_k(-\mathbf{r}, t)$ then there are two distinct solutions which are mirror images of each other.

Let X_{sk} be a stationary solution of Equation (19.2.4). The stability of this state can be analyzed as before by considering the evolution of $X_k = X_{sk} + \delta_k$, where δ_k is a small perturbation. If δ_k decays exponentially,

then the stationary state is stable. This generally happens when λ is less than a 'critical value' λ_c. When λ exceeds λ_c it may happen that the perturbations δ_k, instead of decaying exponentially, grow exponentially, thus making the state X_{sk} unstable. Precisely at λ_c, new solutions to Equation (19.2.4) will appear. As we will see in detail in the following sections, in the vicinity of λ_c, the new solutions often take the form

$$X_k(\mathbf{r}, t;\ \lambda) = X_{sk}(\lambda_c) + \alpha_k \psi_k(\mathbf{r}, t) \tag{19.2.5}$$

in which $X_{sk}(\lambda_c)$ is the stationary state when $\lambda = \lambda_c$, α_k are a set of 'amplitudes' that are to be determined and $\psi_k(r, t)$ are functions that can be obtained from Z_k in Equation (19.2.4). The general theory of bifurcation provides a means of obtaining the time evolution of the amplitudes α_k through a set of equations of the type (see Reference [4] and references therein)

$$\frac{\mathrm{d}\alpha_k}{\mathrm{d}t} = G(\alpha_k, \lambda) \tag{19.2.6}$$

These are called the **bifurcation equations**. In fact, though Equation (19.2.1) is an equation in its own right, it is also a bifurcation equation for systems that break a twofold symmetry. The multiplicity of solutions to Equation (19.2.6) corresponds to the multiplicity of solutions to the original equation (19.2.4).

In this manner, instability, bifurcation, multiplicity of solutions and symmetry are all interrelated. We shall now give a few detailed examples of instability of the thermodynamic branch leading to dissipative structures.

19.3 Chiral Symmetry Breaking and Life

The chemistry of life as we know it is founded on a remarkable asymmetry. A molecule whose geometrical structure is not identical to its mirror image is said to possess **chirality**, or handedness. Mirror-image structures of a chiral molecule are called **enantiomers**. Just as we distinguish the left and the right hand, the two mirror-image structures are identified as L- and D-enantiomers (L for 'levo' and D for 'dextro'; *R* and *S* is another convention of identifying the two enantiomers). Amino acids, the building blocks of proteins, and deoxyribose in DNA are chiral molecules. In the entire biosphere, almost all amino acids that take part in the chemistry of life are L-amino acids (Figure 19.2) and the riboses in DNA and RNA are D-riboses (Figure 19.3). As Francis Crick noted in his book *Life Itself*, 'The first great unifying principle of biochemistry is that the key molecules have the same hand in all organisms.' This is all the more remarkable because chemical reactions show equal preference for the two mirror-image forms (except for very small differences due to parity-nonconserving electroweak interactions [5–7]).

Biochemistry's hidden molecular asymmetry was discovered by Louis Pasteur in 1857. Nearly 150 years later, its true origin remains elusive and it is a subject of active research. Nevertheless, we can see how such a state might be realized in the framework of dissipative structures. First, we note that such an asymmetry can

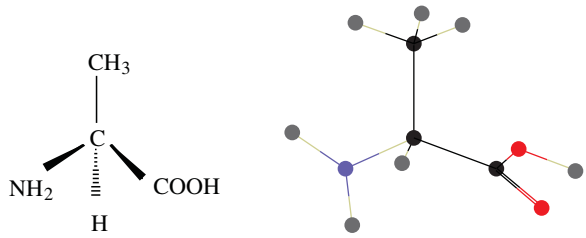

Figure 19.2 *Proteins are made exclusively of L-amino acids. The amino acid shown is L-alanine. In other L-amino acids, different groups of atoms take the place of CH_3.*

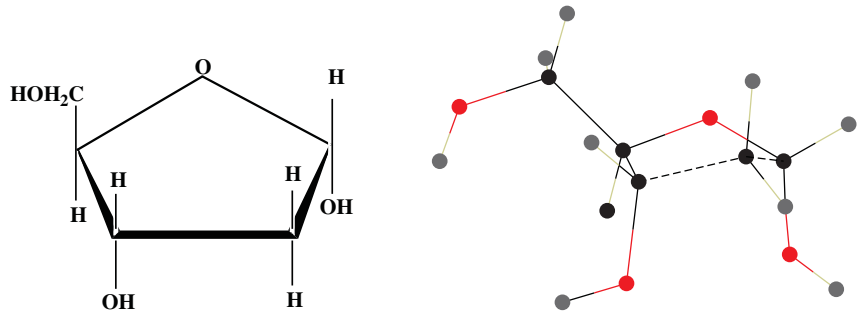

Figure 19.3 *The 2-deoxy-D-ribose shown above is a basic chiral building block of DNA. Its mirror image structure, 2-deoxy-L-ribose, is excluded from the chemistry of life.*

arise only under far-from-equilibrium conditions; at equilibrium, the concentrations of the two enantiomers must be equal. The maintenance of this asymmetry requires constant catalytic production of the preferred enantiomer in the face of interconversion between enantiomers, called **racemization**. (Racemization drives the system to the equilibrium state in which the concentrations of the two enantiomers will become equal.) Second, following the paradigm of order through fluctuations, we will presently see how, in systems with appropriate chiral autocatalysis, the thermodynamic branch, which contains equal amounts of L- and D-enantiomers, can become unstable. The instability is accompanied by the bifurcation of asymmetric states, or states of broken symmetry, in which one enantiomer dominates. Driven by random fluctuations, the system makes a transition to one of the two possible states.

In 1953 F.C. Frank [8] devised a simple model reaction scheme with chiral autocatalysis that could amplify a small initial asymmetry. We shall modify this reaction scheme so that its nonequilibrium aspects, instability and bifurcation of symmetry breaking states can be clearly seen (Figure 19.4). It includes chirally autocatalytic reactions:

$$S + T \underset{k_{1r}}{\overset{k_{1f}}{\rightleftharpoons}} X_L \tag{19.3.1}$$

$$S + T + X_L \underset{k_{2r}}{\overset{k_{2f}}{\rightleftharpoons}} 2X_L \tag{19.3.2}$$

$$S + T \underset{k_{1r}}{\overset{k_{1f}}{\rightleftharpoons}} X_D \tag{19.3.3}$$

$$S + T + X_D \underset{k_{2f}}{\overset{k_{2f}}{\rightleftharpoons}} 2X_D \tag{19.3.4}$$

$$X_L + X_D \underset{k_{3r}}{\overset{k_{3f}}{\rightleftharpoons}} P \tag{19.3.5}$$

Each enantiomer of X is produced directly from the achiral[1] reactants S and T, as shown in reactions (19.3.1) and (19.3.3) and autocatalytically, as shown in reactions (19.3.2) and (19.3.4). In addition, the two enantiomers react with one another and turn into an inactive dimer, P. Due to symmetry, the rate constants for the direct reactions, (19.3.1) and (19.3.3), as well as the autocatalytic reactions, (19.3.2) and (19.3.4), must be equal.

[1]Objects that do not possess a sense of handedness are called achiral. The molecule NH_3 is an example of an achiral molecule.

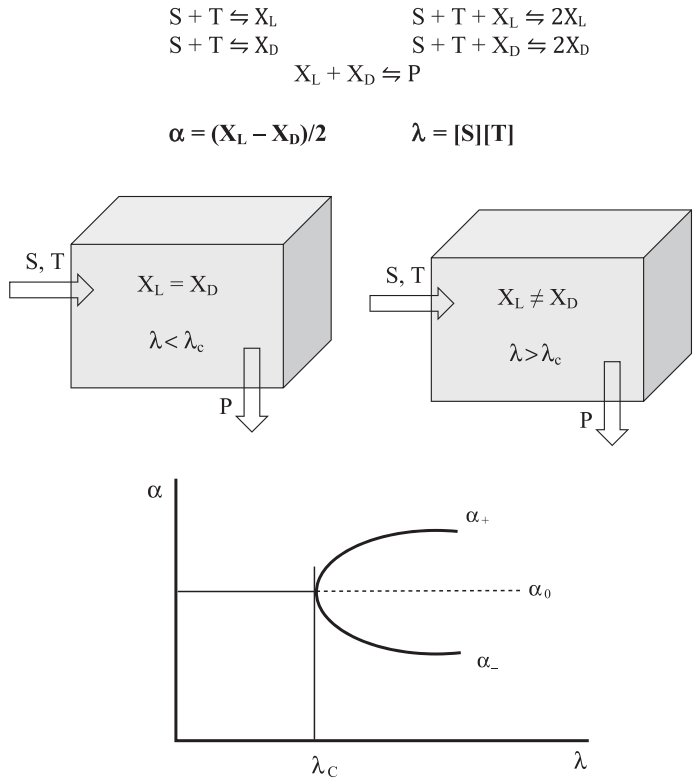

Figure 19.4 *A simple autocatalytic reaction scheme in which X_L and X_D are produced with equal preference. However, in an open system, this leads to a dissipative structure in which $X_L \neq X_D$, a state of broken symmetry. A bifurcation diagram shows some general features of transitions to dissipative structures.*

It is easy to see that, at equilibrium, the system will be in a *symmetric state*, i.e. $[X_L] = [X_D]$ (Exercise 19.3). Now let us consider an open system into which S and T are pumped and from which P is removed. For mathematical simplicity, we assume that the pumping is done in such a way that the concentrations [S] and [T] are maintained at a fixed level, and that due to removal of P the reverse reaction in (19.3.5) may be ignored. Such an approximation does not limit its conclusions in any significant way – as can be seen in the numerical simulations using the *Mathematica* codes that include the reverse reaction (see Appendix 19.1). The kinetic equations of this system are

$$\frac{d[X_L]}{dt} = k_{1f}[S][T] - k_{1r}[X_L] + k_{2f}[X_L][S][T] - k_{2r}[X_L]^2 - k_3[X_L][X_D] \tag{19.3.6}$$

$$\frac{d[X_D]}{dt} = k_{1f}[S][T] - k_{1r}[X_D] + k_{2f}[X_D][S][T] - k_{2r}[X_D]^2 - k_3[X_L][X_D] \tag{19.3.7}$$

Since the equilibrium constants of the direct reaction and the catalyzed reaction should be the same; the rate constants must be such that $(k_{1f}/k_{1r}) = (k_{2f}/k_{2r})$. To make the symmetric and asymmetric states explicit, it is convenient to define the following variables:

$$\lambda = [S][T], \quad \alpha = \frac{[X_L] - [X_D]}{2}, \quad \beta = \frac{[X_L] + [X_D]}{2} \tag{19.3.8}$$

When Equations (19.3.6) and (19.3.7) are rewritten in terms of α and β (Exercise 19.4), we have

$$\frac{d\alpha}{dt} = -k_{1r}\alpha + k_{2f}\lambda\alpha - 2k_{2r}\alpha\beta \tag{19.3.9}$$

$$\frac{d\beta}{dt} = k_{1f}\lambda - k_{1r}\beta - k_{2f}\lambda\beta - k_{2r}(\beta^2 + \alpha^2) - k_3(\beta^2 - \alpha^2) \tag{19.3.10}$$

The stationary states of these equations can be obtained after a little calculation (by setting $d\alpha/dt = d\beta/dt = 0$). A complete analytic study of the solutions of Equations (19.3.9) and (19.3.10) and their stability is somewhat lengthy and can be found in the literature [4]. We shall only state the main results of this analysis. With the *Mathematica* code provided in Appendix 19.1, the reader can explore the properties of the equation quite easily and verify the phenomenon of chiral symmetry breaking in this system (Figure 19.5).

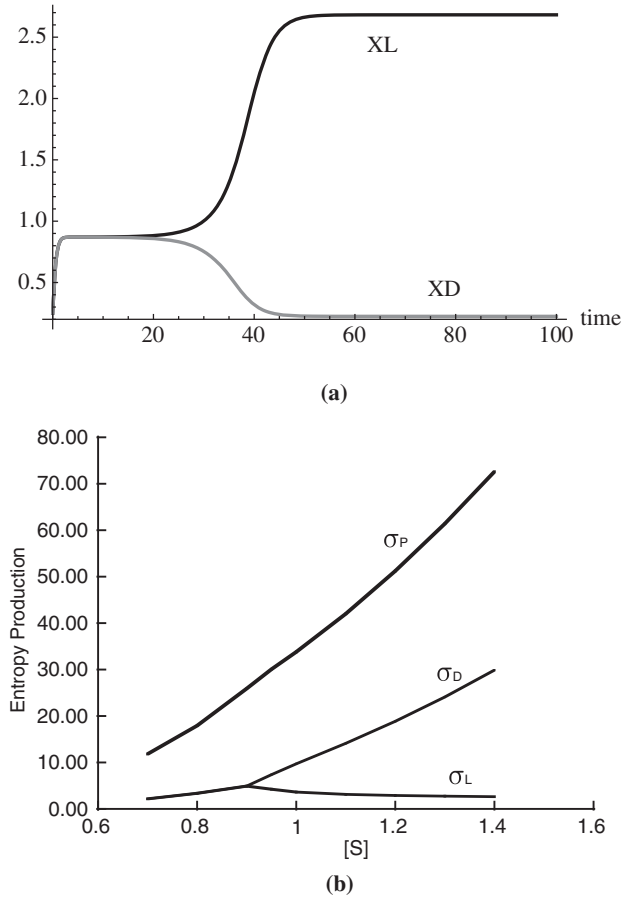

Figure 19.5 *(a) Time evolution of X_L and X_D obtained using* Mathematica *Code A given in Appendix 19.1. For $\lambda > \lambda_c$ a small initial fluctuation in X_L grows to establish a state of broken symmetry in which the concentrations of X_L and X_D are unequal. (b) Steady-state entropy production in the reaction model (19.3.1) to (19.3.5) as a function of [S], where σ_P is the entropy production due to reaction (19.3.5), σ_D is the entropy production due to reaction (19.3.3) and (19.3.4) and σ_L is the entropy production due to reactions (19.3.1) and (19.3.2). The numerical values used in the model are: $k_{1f} = 0.5$; $k_{1r} = 0.2$; $k_{2f} = 0.5$; $k_{2r} = (k_{1r}/k_{1f})k_{2f}$; $k_{3f} = 1.5$; $k_{3r} = 10^{-3}$; [P] = 0.5; [T] = [S], and [S] varies in the shown range.*

For small values of λ the stable stationary state is

$$\alpha_s = 0 \tag{19.3.11}$$

$$\beta_s = \frac{2k_{2r}\beta_a + \sqrt{(2k_{2r}\beta_a)^2 + 4(k_{2r} + k_3)k_{1f}\lambda}}{2(k_{2r} + k_3)} \tag{19.3.12}$$

in which

$$\beta_a = \frac{k_{2f}\lambda - k_{1r}}{2k_{2r}}$$

This is a *symmetric* solution in which $[X_L] = [X_D]$ (as indicated by the subscript s). Using the stability analysis described in the previous chapter, it can be shown that this symmetric solution becomes unstable when λ is greater than a critical value λ_c. The value of λ_c is given by

$$\lambda_c = \frac{s + \sqrt{s^2 - 4k_{2f}^2 k_{1r}^2}}{2k_{2f}^2} \tag{19.3.13}$$

where

$$s = 2k_{2f}k_{1r} + \frac{4k_{2r}^2 k_{1r}}{k_3 - k_{2r}} \tag{19.3.14}$$

For the system of equations (19.3.9) and (19.3.10) it is possible to obtain an asymmetric stationary solution analytically:

$$\alpha_a = \pm\sqrt{\beta_a^2 - \frac{k_{1f}\lambda}{k_3 - k_{2r}}} \tag{19.3.15}$$

$$\beta_a = \frac{k_{2f}\lambda - k_{1r}}{2k_{2r}} \tag{19.3.16}$$

in which the subscript a stands for *asymmetric*. (We recommend the reader to use *Mathematica* code A in Appendix 19.1 to verify all these properties of the system.)

The simplest process that demonstrates chiral symmetry breaking is in the crystallization of $NaClO_3$ under far-from-equilibrium conditions [9]. During the last two decades, other chirally autocatalytic reactions were discovered through the mechanism of catalysis in these systems but are not as simple as the one presented in the above model [10]. These chirally autocatalytic reactions are capable of amplifying extremely small initial asymmetries. The simple model, however, leads to interesting conclusions regarding the sensitivity of bifurcation discussed below.

19.3.1 Entropy Production Is Chiral-Symmetry-Breaking Transitions

Dissipative structures are generated and maintained through irreversible processes that continuously generate entropy. Let us look at the entropy generation in the model system studied above. We assume each of the reactions (19.3.1) to (19.3.5) is an elementary step so that we can use the formula $(1/V)\mathrm{d}S/\mathrm{d}t = R(R_f - R_r)\ln(R_f/R_r)$, which gives the rate of entropy generated per unit volume by that reaction (see Equation (9.5.10); here R_f and R_r are the forward and reverse reaction rates and R is the gas constant. Though in the theoretical analysis we have ignored the reverse reaction (19.3.5), we shall include it in calculating the rate of entropy production to make the affinity of this reaction finite.

Using the numerical values specified in the caption of Figure 19.3b, we calculate the entropy production for each of the reactions in the above model. Our objective is to investigate how the rate of entropy production changes when the system moves from a region below the critical point, where system evolves to a symmetric steady state $[X_L] = [X_D]$, to a region above the critical point, where the system evolves to an asymmetric state, $[X_L] \neq [X_D]$. The values of [S], [T] and [P] are the parameters of the system. Keeping [P] at a fixed value and setting [S] = [T], we obtain the steady-state rates of entropy production of each of the reactions in the model. We do the same for various values of [S] and tabulate the entropy production rates for each value of [S]. The range of values of [S] extends from the region below the critical point to a value above the critical point. Salient features of the results are shown graphically in Figure 19.5b. This graph shows the entropy production due to the reactions that produce X_L, (19.3.1) and (19.3.2), as σ_L; similarly, σ_D is the corresponding entropy production for X_D. The entropy production due to the reaction that produces P is indicated as σ_P. The behavior of σ_L and σ_D is interesting: both increase identically till [S] reaches the critical point and then they diverge. The entropy production due to the dominant X_L decreases above the critical point while that of X_D continues to increase. This indicates that the dominant species, X_L, is closer to its equilibrium value compared with X_D; through the reaction $X_L + X_D \rightleftharpoons P$, the dominant X_L keeps the concentration of X_D at a low value and farther away from its equilibrium value. The bulk of the total entropy production of the system comes from the reaction producing P, as σ_P indicates. Furthermore, for the above model, by artificially making $X_L = X_D$ above the critical point one can show that the entropy production is lower for the asymmetric state. Thus, when the unstable symmetric state makes a transition to the asymmetric state above the critical point, then entropy production decreases. The rate of entropy production is in general not a widely studied topic. We encourage the reader to explore this aspect of nonequilibrium systems.

19.3.2 Nonequilibrium Symmetry Breaking and the Origin of Biomolecular Asymmetry

The above example shows how a far-from-equilibrium chemical system can generate and maintain chiral asymmetry, but it only provides a general framework in which we must seek the origins of biomolecular handedness. The origin of biomolecular handedness, or life's **homochirality**, remains to be explained [11,12]. Here we shall confine our discussion to how the theory of nonequilibrium symmetry breaking contributes to this important topic. We cannot yet say with confidence whether chiral asymmetry arose in a prebiotic (i.e. before life) process and facilitated the evolution of life, or whether some primitive form of life that incorporated both L- and D-amino acids arose first and subsequent evolution of this life form led to the homochirality of L-amino acids and D-sugars. Both views have their proponents.

A related question is whether the dominance of L-amino acids in biochemistry was a matter of chance or whether it was a consequence of the extremely small but systematic chiral asymmetry due to electroweak interactions that are known to exist at the atomic and molecular levels [5–7, 13, 14]. Theories that support both views have been put forward but there is no general consensus on this matter either, mainly because there is a dearth of persuasive experimental evidence. However, the theory of nonequilibrium symmetry breaking provides a valuable means of assessing the plausible role of different models. For example, if we consider a prebiotic symmetry-breaking process that might have occurred in the oceans, it is possible to develop a general theory of symmetry breaking. A parameter λ, similar to the one in the above model, can be defined for any symmetry-breaking system. When $\lambda < \lambda_c$, the system will be in a symmetric state; for $\lambda > \lambda_c$ the symmetric state will become unstable and evolve to an asymmetric state. Furthermore, regardless of the complexities of the reaction scheme, based only on symmetry considerations, it is possible to describe the bifurcation of the chiral symmetry-breaking states with an equation of the following type [15, 16]:

$$\frac{d\alpha}{dt} = -A\alpha^3 + B(\lambda - \lambda_c)\alpha + Cg + \sqrt{\varepsilon f(t)} \tag{19.3.17}$$

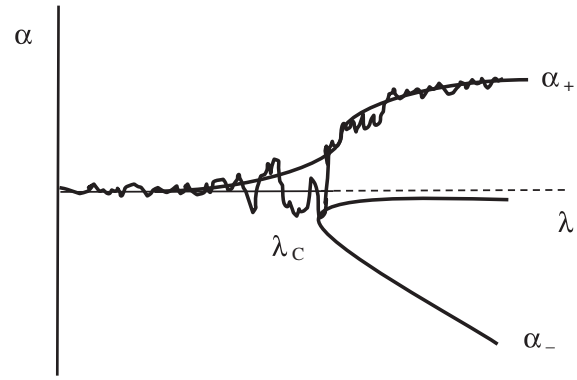

Figure 19.6 *A symmetry-breaking transition or bifurcation in the presence of a small bias that favors one of the bifurcating branches. It can be analyzed through the general equation (19.3.17) and the probability of the system making a transition to the favored branch is given by Equation (19.3.18).*

in which the coefficients A, B and C depend on the concentrations of the reactants and on the reaction rates (Figure 19.6). The parameter g is a small systematic bias, such as due to the electroweak force [6, 14] or other systematic chiral influences such as spin-polarized electrons that emerge from radioactive decay [17], or circularity polarized electromagnetic radiation emitted by certain stars that might fill large regions of space for long periods of time [11]. The systematic influence appears in the form of the rates of production or destruction of one enantiomer being larger than that of the other. The term $\sqrt{\varepsilon f(t)}$ represents random fluctuations with the root-mean-square value $\sqrt{\varepsilon}$. Since the assumptions about rates of production for biomolecules, their catalytic activities and their concentrations determine the coefficients A, B and C, rather than the details of the chemical reaction scheme, the model is constrained by our general understanding of the prebiotic chemistry. Equation (19.3.17) provides a way to assess whether a given prebiotic model can produce and maintain the required asymmetry in a reasonable amount of time.

Furthermore, Equation (19.3.17) can also give us a quantitative measure for the systematic chiral influence g. Detailed analysis [16, 18] of this equation has shown that the sensitivity of the bifurcation to the systematic influence depends on the rate at which the system moves through the critical point λ_c; i.e. we assume that $\lambda = \lambda_0 + \gamma t$, so that the initial value of λ_0 is less than λ_c, but that λ gradually increases to a value larger than λ_c at an average rate γ. This process may correspond, for example, to a slow increase in the concentrations of biomolecules in the oceans. It has been shown [16, 18] that the probability P of the system making a symmetry-breaking transition to the asymmetric state favored by the systematic chiral influence g is given by

$$P = \frac{1}{\sqrt{2\pi}} \int_{-\infty}^{N} \mathrm{e}^{-x^2/2} \mathrm{d}x \quad \text{where} \quad N = \frac{\mathrm{Cg}}{\sqrt{\varepsilon/2}} \left(\frac{\pi}{B\gamma} \right)^{1/4} \tag{19.3.18}$$

Although *derived in the context of biomolecular handedness, this formula is generally valid for any system that breaks a twofold symmetry, such as mirror inversion*. Using this formula, it is possible to understand the extraordinary sensitivity of bifurcation to small systematic biases that favor one enantiomer by increasing its production rate. Calculations show that L-amino acids have a lower ground-state energy [14]. For example, it can be estimated that the chiral asymmetry of the electroweak interaction can create differences of the order of one part in 10^{17} between the production rates of the enantiomers. Application of the above theory shows that if the autocatalytic production rate of the chiral molecules is faster than the racemization rates, then for a period in the range 10^4 to 10^5 years, the enantiomer favored by the electroweak force will dominate [16].

For such a scenario, there is currently no experimental evidence to show us how chiral autocatalysis with the required properties can originate in prebiotic chiral molecules.

Many different scenarios have been suggested for the possible origins of biomolecular handedness. An extensive review can be found in the literature [19]. Note that, even if one is considering a process of chiral asymmetry generation after 'life' arose, equations of the type (19.3.17) can still be used to describe the symmetry-breaking process, but this time the model will contain as 'reactants' the self-replicating unit of life.

19.4 Chemical Oscillations

Our next example of a dissipative structure illustrates how the breaking of time-translation symmetry leads to oscillatory behavior. Some early reports of concentration oscillations were discounted because it was widely believed that such behavior was not consistent with thermodynamics. That is why the report on oscillating reactions by Bray in 1921 and Belousov in 1958 were met with skepticism [20]. Although it is true that oscillations of the extent of reaction ξ about its equilibrium value will violate the Second Law, oscillations of concentration about a nonequilibrium value of ξ do not violate the Second Law. When it was realized that systems far from thermodynamic equilibrium could exhibit oscillations, interest in these and other oscillating reactions rose sharply and gave rise to a rich study of dissipative structures in chemical systems.

Developments in the theoretical understanding of instability for nonequilibrium states in the 1960s [3] stimulated the experimental study of autocatalytic chemical kinetics that could give rise to concentration oscillations through the phenomenon of bifurcation. In 1968 Prigogine and Lefever [21] developed a simple model that not only demonstrated clearly how a nonequilibrium system can become unstable and make a transition to an oscillatory state, but also proved to be a rich source for theoretical understanding of propagating waves and almost every other phenomenon observed in real chemical systems, most of which are extremely complex to study. Due to its impact on the study of dissipative structures, it is often called the **Brusselator** (after its place of origin, the Brussels School of Thermodynamics) or the 'trimolecular model' due to the trimolecular autocatalytic step in the reaction scheme. Because of its theoretical simplicity, we shall discuss this reaction first and then present the experimentally studied Belousov–Zhabotinsky reaction. The Brusselator reaction scheme and the corresponding rates are:

$$\mathrm{A} \xrightarrow{k1} \mathrm{X}, \qquad \mathrm{k}_1[\mathrm{A}] \tag{19.4.1}$$

$$\mathrm{B} + \mathrm{X} \xrightarrow{k2} \mathrm{Y} + \mathrm{D}, \qquad \mathrm{k}_2[\mathrm{B}][\mathrm{X}] \tag{19.4.2}$$

$$2\mathrm{X} + \mathrm{Y} \xrightarrow{k3} 3\mathrm{X}, \qquad \mathrm{k}_3[\mathrm{X}]^2[\mathrm{Y}] \tag{19.4.3}$$

$$\mathrm{X} \xrightarrow{k4} \mathrm{E}, \qquad \mathrm{k}_4[\mathrm{X}] \tag{19.4.4}$$

The net reaction of this scheme is $\mathrm{A} + \mathrm{B} \rightarrow \mathrm{D} + \mathrm{E}$. We assume that the concentrations of the reactants A and B are maintained at a desired nonequilibrium value through appropriate flows. The products D and E are removed as they are formed. We also assume that the reaction occurs in a solution that is well stirred and hence homogeneous. If we further assume that all the reverse reactions are so slow they can be neglected, we have the following rate equations for the species X and Y:

$$\frac{\mathrm{d}[\mathrm{X}]}{\mathrm{d}t} = k_1[\mathrm{A}] - k_2[\mathrm{B}][\mathrm{X}] + k_3[\mathrm{X}]^2[\mathrm{Y}] - k_4[\mathrm{X}] \equiv Z_1 \tag{19.4.5}$$

$$\frac{\mathrm{d}[\mathrm{Y}]}{\mathrm{d}t} = k_2[\mathrm{B}][\mathrm{X}] - k_3[\mathrm{X}]^2[Y] \equiv Z_2 \tag{19.4.6}$$

One can easily verify (Exercise 19.5) that the stationary solutions, $[X]_s$ and $[Y]_s$, to these equations are

$$[X]_s = \frac{k_1}{k_4}[A], \quad [Y]_s = \frac{k_4 k_2}{k_3 k_1}\frac{[B]}{[A]} \tag{19.4.7}$$

As was explained in Section 18.4, the stability of the stationary state depends on the eigenvalues of the Jacobian matrix

$$\begin{bmatrix} \dfrac{\partial Z_1}{\partial [X]} & \dfrac{\partial Z_1}{\partial [Y]} \\ \dfrac{\partial Z_2}{\partial [X]} & \dfrac{\partial Z_2}{\partial [Y]} \end{bmatrix} \tag{19.4.8}$$

evaluated at the stationary state (19.4.7). The explicit form of the Jacobian matrix that was derived in Chapter 18 is (see Equation (18.4.13)):

$$\begin{bmatrix} k_2[B] - k_4 & k_3[X]_s^2 \\ -k_2[B] & -k_3[X]_s^2 \end{bmatrix} = M \tag{19.4.9}$$

The example in Section 18.4 shows how the stationary state (19.4.7) becomes unstable when a complex conjugate pair of eigenvalues of the matrix M cross the imaginary axis; for the Brusselator this happens when

$$[B] > \frac{k_4}{k_2} + \frac{k_3 k_1^2}{k_2 k_4^2}[A]^2 \tag{19.4.10}$$

The system makes a transition to an oscillatory state and the resulting oscillations are shown in Figure 19.7. The steady states and the transition to oscillations can easily be investigated using the *Mathematica* codes provided in Appendix 19.1.

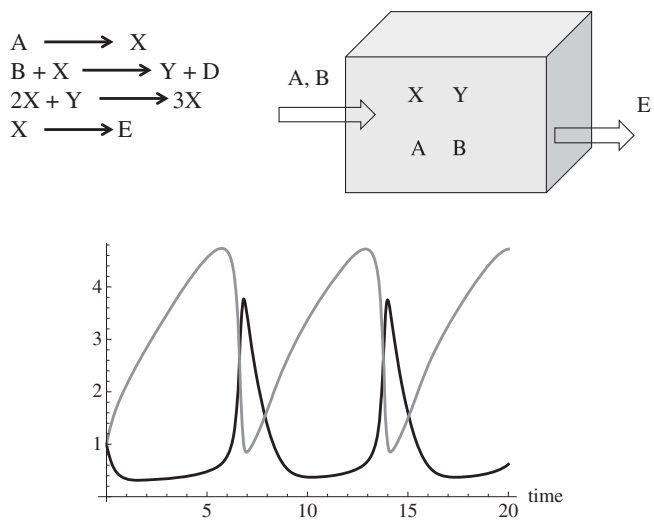

Figure 19.7 *Brusselator model, model flow reactor and oscillations in [X] and [Y] obtained using* Mathematica *in Appendix 19.1.*

19.4.1 The Belousov–Zhabotinsky Reaction

Once it became clear that concentration oscillations are not inconsistent with the laws of thermodynamics (as the theoretical models of oscillating reactions showed), interest grew in the neglected 1958 report by Belousov and the later experiments of Zhabotinsky reported in a 1964 article [22]. These experimental studies of Belousov and Zhabotinsky were conducted in the Soviet Union and made known to the Western world through the Brussels School of Thermodynamics. In the United States, the study of the Belousov–Zhabotinsky oscillations was taken up by Field, Körös and Noyes [23], who performed a through-study of the reaction mechanism in the early 1970s. This was an important landmark in the study of oscillating reactions. Field, Körös and Noyes identified the key steps in the rather complex **Belousov–Zhabotinsky reaction** and developed a model – which we shall refer to as the **FKN model** – consisting of only three variables that showed how the oscillations arise.

The Belousov–Zhabotinsky reaction is basically catalytic oxidation of an organic compound such as malonic acid, $CH_2(COOH)_2$. The reaction occurs in an aqueous solution and is easily performed in a beaker by simply adding the following reactants in the concentrations shown:

$$[H^+] = 2.0\,\mathrm{M} \quad [CH_2(COOH)_2] = 0.28\,\mathrm{M}$$
$$[BrO_3{}^-] = 6.3 \times 10^{-2}\mathrm{M} \quad [Ce^{4+}] = 2.0 \times 10^{-3}\mathrm{M}$$

After an initial 'induction' period, the oscillatory behavior can be seen in the variation of the concentration of the Ce^{4+} ion, due to which there is a change in color from colorless to yellow. Many variations of this reaction – with more dramatic variations of color – are known today. (A wealth of detail about the Belousov–Zhabotinsky may be found in the literature [24].)

Box 19.1 presents a simplified version of the reaction mechanism from which the FKN model was developed. Later models of the Belousov–Zhabotinzky reactions have included as many as 22 reaction steps. The FKN model of the Belousov–Zhabotinsky reaction makes the following identifications: $A = BrO_3{}^-$, $X = HBrO_2$, $Y = Br^-$, $Z = Ce^{4+}$, $P = [HBrO]$ and $B = [Org]$, an organic species that is oxidized. In modeling the reaction, $[H^+]$ is absorbed in the definition of the rate constant. The reaction scheme consists of the following steps and corresponding rates:

- Generation of $HBrO_2$

$$A + Y \rightarrow X + P, \qquad k_1[A][Y] \tag{19.4.11}$$

- Autocatalytic production of $HBrO_2$

$$A + X \rightarrow 2X + 2Z, \qquad k_2[A][X] \tag{19.4.12}$$

- Consumption of $HBrO_2$

$$X + Y \rightarrow 2P, \qquad k_3[X][Y] \tag{19.4.13}$$

$$2X \rightarrow A + P, \qquad k_4[X]^2 \tag{19.4.14}$$

- Oxidation of the organic reactants

$$B + Z \rightarrow (f/2)Y, \qquad k_5[B][Z] \tag{19.4.15}$$

Box 19.1 The Belousov–Zhabotinsky reaction and the FKN model

The Field–Köros–Noyes (FKN) model of the Belousov–Zhabotinsky reaction consists of the following steps with A = BrO_3^-, X = $HBrO_2$, Y = Br^-, Z = Ce^{4+}, P = HBrO and B = Org. In modeling the reaction, $[H^+]$ is absorbed in the definition of the rate constant.

- Generation of $HBrO_2$: A + Y → X + P

$$BrO_3^- + Br^- + 2H^+ \rightarrow HBrO_2 + HBrO \tag{1}$$

- Autocatalytic production of $HBrO_2$: A + X → 2X + 2Z

$$BrO_3^- + HBrO_2 + H^+ \rightarrow 2BrO_2 + H_2O \tag{2}$$

$$BrO_2 + Ce^{3+} + H^+ \rightarrow HBrO_2 + Ce^{4+} \tag{3}$$

The net reaction, (2) + 2(3), is autocatalytic in $HBrO_2$. Since the rate-determining step is (2), the reaction is modeled as $BrO_3^- + HBrO_2 \xrightarrow{H+,Ce^{3+}} + 2Ce^{4+} + 2HBrO_2$

- Consumption of $HBrO_2$: X + Y → 2P and 2X → A + P

$$HBrO_2 + Br^- + H^+ \rightarrow 2HBrO \tag{4}$$

$$2HBrO_2 \rightarrow BrO_3^- + HBrO + H^+ \tag{5}$$

- Oxidation of the organic reactants: B + Z → (*f*/2)Y

$$CH_2(COOH)_2 + Br_2 \rightarrow BrCH(COOH)_2 + H^+ + Br^- \tag{6}$$

$$CH^{4+} + \frac{1}{2}[CH_2(COOH)_2 + BrCH(COOH)_2 \rightarrow \frac{f}{2}Br^- + Ce^{3+} + \text{Products} \tag{7}$$

The oxidation of the organic species is a complex reaction. It is approximated by a single rate determining step (7). In the FKN model, concentration [B] of the organic species is assumed to be constant. The value of the effective stoichiometric coefficient *f* is a variable parameter. Oscillations occur if *f* is in the range 0.5–2.4.

The corresponding rate equations are

$$\frac{d[X]}{dt} = k_1[A][Y] + k_2[A][X] - k_3[X][Y] - 2k_4[X]^2 \tag{19.4.16}$$

$$\frac{d[Y]}{dt} = -k_1[A][Y] - k_3[X][Y] + \frac{f}{2}k_5[B][Z] \tag{19.4.17}$$

$$\frac{d[Z]}{dt} = 2k_2[A][X] - k_5[B][Z] \tag{19.4.18}$$

Stationary states of this equation can be found after a little calculation (Exercise 19.7). To study its stability involves analyzing the roots of a third-degree equation. There are many analytical methods [25] to analyze the oscillatory behavior of such a system, but these details are outside our main objective of giving examples of oscillating chemical systems. The oscillatory behavior of these equations may be numerically studied quite

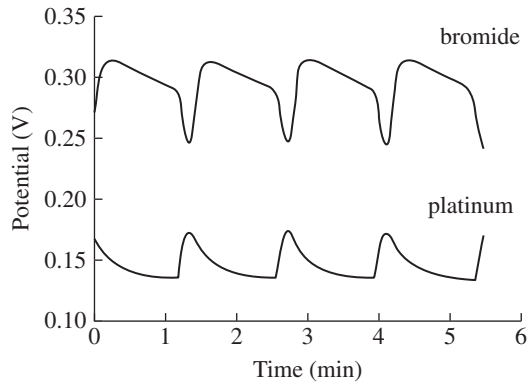

Figure 19.8 *Experimentally observed oscillations in [Br^-] for the Belousov–Zhabotinsky reaction; the concentrations were measured using electrodes. (Courtesy of John Pojman.)*

easily using *Mathematica* Code C in Appendix 19.1 (Figures 19.8 and 19.9). For numerical solutions, one may use the following data [25]:

$$k_1 = 1.28\,\text{mol}^{-1}\,\text{L}\,\text{s}^{-1}, k_2 = 8.0\,\text{mol}^{-1}\,\text{L}\,\text{s}^{-1}, \quad k_3 = 8.0 \times 10^5\,\text{mol}^{-1}\,\text{L}\,\text{s}^{-1}$$
$$k_4 = 2.0 \times 10^3\,\text{mol}^{-1}\,\text{L}\,\text{s}^{-1}, \quad k_5 = 1.0\,\text{mol}^{-1}\text{L}\,\text{s}^{-1}$$
$$[\text{B}] = [\text{Org}] = 0.02\text{M}, \quad [\text{A}] = [\text{BrO}_3{}^-] = 0.06\text{M}, \quad 0.5 < f < 2.4 \tag{19.4.19}$$

The Belousov–Zhabotinsky reaction shows oscillations of great variety and complexity; it even exhibits chaos. In chaotic systems arbitrarily close initial conditions diverge exponentially; the system exhibits aperiodic behavior. A review by Epstein and Showalter [26] summarizes these aspects. It also produces propagating waves and multistability. A large number of very interesting phenomena have been studied using this reaction [24, 25].

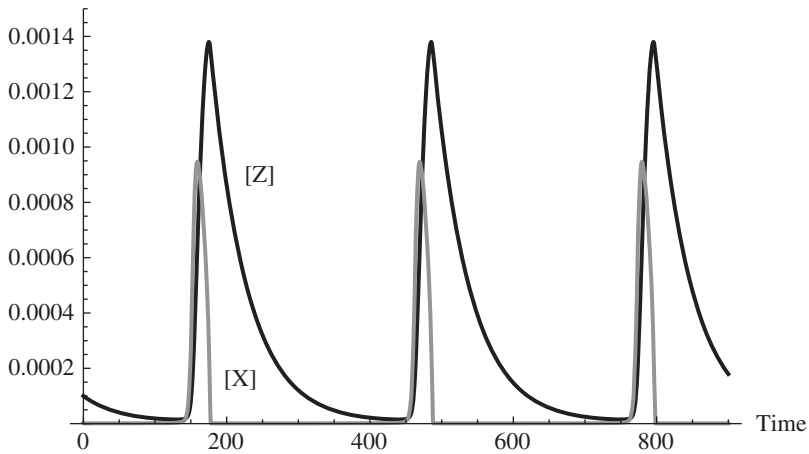

Figure 19.9 *Oscillatory solutions obtained numerically using the FKN model of the Belousov–Zhabotinsky reaction: [X] = [$HBrO_2$] and [Z] = [Ce^{4+}]. The plots were obtained using* Mathematica *codes in Appendix 19.1.*

19.4.2 Other Oscillating Reactions

During the last two decades, many more oscillating chemical reactions have been discovered. Indeed, Irving Epstein and coworkers in the United States [27–29] and De Kepper and Boissonade in France [30] developed a systematic way of designing oscillating chemical reactions. In biochemical systems, one of the most interesting oscillating behaviors is found in the glycolytic reaction. A recent monograph by Albert Goldbeter [31] summarizes the vast amount of study on oscillatory biochemical systems.

19.5 Turing Structures and Propagating Waves

From the delicate beauty of the butterfly to the 'fearful symmetry' of the tiger, Nature if full of wondrous patterns, both animate and inanimate. How do these patterns arise? Dissipative processes in systems far from thermodynamic equilibrium may provide at least a partial answer.

The emergence of biological morphology during embryonic development – with hands and feet and eyes all in the right place – is a fascinating subject (a popular account of this subject is Lewis Wolperts's *Triumph of the Embryo*, 1991, Oxford University Press). What mechanism produces the morphology of living organisms? In 1952 the British mathematician Alan Turing suggested a mechanism based on the processes of chemical reactions and diffusion [32]. He showed, by devising a simple model, how chemical reactions and diffusion can work in consonance to produce stable stationary patterns of concentrations. Turing proposed it to explain biological morphogenesis. Today we know that biological morphogenesis is a very complex process, too complex to be explained entirely by the processes of diffusion and chemical reactions. However, Turing's observation has gained much attention since the 1970s due to the great interest in theoretical and experimental study of far-from-equilibrium chemical systems. In this section we will briefly describe a **Turing structure**, or a stationary **spatial dissipative structure**, using the Brusselator of Section 19.4.

For simplicity, we shall consider a system with one spatial dimension, with coordinate r, in which diffusion occurs (Figure 19.10). We assume the system extends from $-L$ to $+L$. We must also specify spatial boundary conditions; the usual boundary conditions are that either the concentrations of the reactants or their flows are maintained at a constant value at the boundaries (or even a combination of both). For our example, we shall assume that the flows of the reactants are zero at the boundaries. Since diffusion flow is proportional to the derivative $\partial C/\partial r$ (in which C is the concentration), the no-flow boundary conditions imply that the derivatives of the concentrations are zero at the boundaries.

When diffusion is included as a transport process, the kinetic equations (19.4.5) and (19.4.6) become

$$\frac{\partial[\mathrm{X}]}{\partial t} = D_{\mathrm{X}}\frac{\partial^2[\mathrm{X}]}{\partial r^2} + k_1[\mathrm{A}] - k_2[\mathrm{B}][\mathrm{X}] + k_3[\mathrm{X}]^2[\mathrm{Y}] - k_4[\mathrm{X}] \tag{19.5.1}$$

$$\frac{\partial[\mathrm{Y}]}{\partial t} = D_{\mathrm{Y}}\frac{\partial^2[\mathrm{Y}]}{\partial r^2} + k_2[\mathrm{B}][\mathrm{X}] - k_3[\mathrm{X}]^2[\mathrm{Y}] \tag{19.5.2}$$

The boundary conditions are

$$\left.\frac{\partial[\mathrm{X}]}{\partial r}\right|_{r=-L} = \left.\frac{\partial[\mathrm{X}]}{\partial r}\right|_{r=+L} = 0$$

in which D_{X} and D_{Y} are the diffusion coefficients and r is the spatial coordinate. As before, we assume that [A] and [B] are maintained at a fixed uniform value along the entire system (an assumption that simplifies the mathematics but which is difficult to achieve in practice). Diffusion usually homogenizes the concentration in a system, but when coupled with autocatalytic chemical reactions under far-from-equilibrium conditions, it actually generates inhomogeneities or patterns. For pattern formation, the diffusion coefficients must be different. If the diffusion coefficients are nearly equal, then diffusion does not cause an instability; diffusion

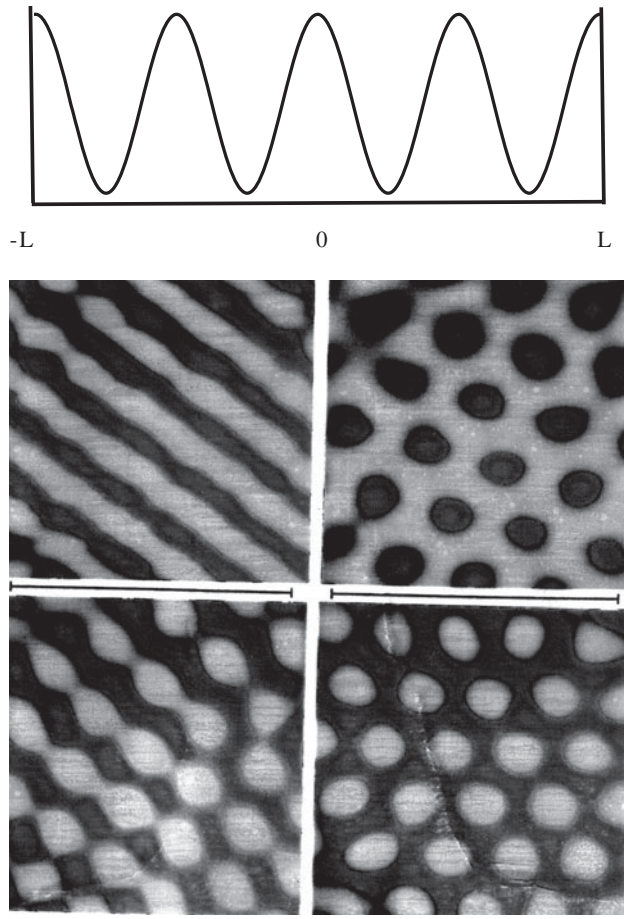

Figure 19.10 *Above: Turing structure in a one-dimensional Brusselator model. Below: Turing structures observed in a chlorite–iodide–malonic acid reaction in an acidic aqueous solution (Courtesy of Harry L. Swinney). The size of each square is nearly 1 mm.*

only tends to homogenize the instability that already exists. This can be seen as follows. We begin by considering the stability of the stationary state (19.4.7), the concentrations being homogeneous in the entire system:

$$[\mathrm{X}]_\mathrm{s} = \frac{k_1}{k_4}\,[\mathrm{A}], \quad [\mathrm{Y}]_\mathrm{s} = \frac{k_4 k_2}{k_3 k_1}\frac{[\mathrm{B}]}{[\mathrm{A}]} \tag{19.5.3}$$

The stability of this solution depends on the behavior of a small perturbation. If δX and δY are the small perturbations from $[\mathrm{X}]_\mathrm{s}$ and $[\mathrm{Y}]_\mathrm{s}$, it is easy to see that equations linearized about the steady state (19.5.3) are

$$\frac{\partial}{\partial t}\begin{pmatrix}\delta X\\ \delta Y\end{pmatrix} = \begin{bmatrix} D_\mathrm{X}\dfrac{\partial^2}{\partial r^2} & 0 \\ 0 & D_\mathrm{Y}\dfrac{\partial^2}{\partial r^2}\end{bmatrix}\begin{pmatrix}\delta X\\ \delta Y\end{pmatrix} + M\begin{pmatrix}\delta X\\ \delta Y\end{pmatrix} \tag{19.5.4}$$

in which we have used the matrix defined in (19.4.9):

$$M = \begin{bmatrix} k_2[\mathrm{B}] - k_4 & k_3[\mathrm{X}]_s^2 \\ -k_2[\mathrm{B}] & -k_3[\mathrm{X}]_s^2 \end{bmatrix}$$

We will first see that a spatial structure will not arise when the diffusion coefficients are equal. If we assume $D_X = D_Y = D$, Equation (19.5.4) can be written as

$$\frac{\partial}{\partial t}\begin{pmatrix} \delta X \\ \delta Y \end{pmatrix} = D\frac{\partial^2}{\partial r^2} I \begin{pmatrix} \delta X \\ \delta Y \end{pmatrix} + M \begin{pmatrix} \delta X \\ \delta Y \end{pmatrix} \tag{19.5.5}$$

in which I is the identity matrix. For a *linear equation* of this type, the spatial part of the solutions can always be written as combinations of Sin Kr and Cos Kr, in which the wavenumbers K are chosen so that the boundary conditions are satisfied. This means that if we understand the behavior of a perturbation of the type

$$\begin{pmatrix} \delta X(t) \\ \delta Y(t) \end{pmatrix} \mathrm{Sin}\, Kr \text{ and } \begin{pmatrix} \delta X(t) \\ \delta Y(t) \end{pmatrix} \mathrm{Cos}\, Kr \tag{19.5.6}$$

in which the spatial part is separated, then the behavior of all linear combinations of these basic solutions can be deduced. If we substitute (19.5.6) into (19.5.5), we obtain

$$\frac{\partial}{\partial t}\begin{pmatrix} \delta X(t) \\ \delta Y(t) \end{pmatrix} = (-DK^2 I + M) \begin{pmatrix} \delta X(t) \\ \delta Y(t) \end{pmatrix} \tag{19.5.7}$$

From this expression, it is clear that if λ_+ and λ_- are the eigenvalues of M, the addition of diffusion will only change the eigenvalues to $(\lambda_+ - DK^2)$ and $(\lambda_- - DK^2)$. Since it is the positivity of the real part of the eigenvalue that indicates instability, we see that diffusion does not generate a new instability; it only makes steady states more stable to perturbations with $K \neq 0$. So the solution to Equation (19.5.7) with $K = 0$ is the least stable state because its eigenvalues will have the largest real parts.

For the emergence of spatial patterns, the diffusion coefficients must be *unequal.* In a small region, if one species diffuses out more rapidly than the other, the growth of one species may be facilitated by the depletion of the other. If this happens, the homogeneous state will no longer be stable and inhomogeneities will begin to grow. When the diffusion coefficients are unequal, it is easy to see that in place of the matrix $(-K^2DI + M)$ we have the matrix

$$\begin{bmatrix} k_2[\mathrm{B}] - k_4 - K^2 D_\mathrm{X} & k_3[\mathrm{X}]_s^2 \\ -k_2[\mathrm{B}] & -k_3[\mathrm{X}]_s^2 - K^2 D_\mathrm{Y} \end{bmatrix} \tag{19.5.8}$$

For an instability to produce stationary **spatial structures**, the two eigenvalues of this matrix must be real and at least one must become positive. If the eigenvalues are real and one becomes positive due to the variations in the parameters [B] and [A], then the unstable perturbation will be of the form

$$\begin{pmatrix} c_1 \\ c_2 \end{pmatrix} \mathrm{Sin}(Kr)\mathrm{e}^{\lambda_+ t} \text{ or } \begin{pmatrix} c_1 \\ c_2 \end{pmatrix} \mathrm{Cos}(Kr)\mathrm{e}^{\lambda_+ t} \tag{19.5.9}$$

in which λ_+ is the eigenvalue with a positive real part. This indicates a growth of a spatial pattern sin Kr or cos Kr without any temporal oscillations; it will evolve to a stationary pattern or a Turing structure.

On the other hand, if the eigenvalues are a complex–conjugate pair, then the solutions to the perturbation equation (19.5.4) will be of the form

$$\begin{pmatrix} c_1 \\ c_2 \end{pmatrix} \mathrm{Sin}(Kr)\mathrm{e}^{(\lambda_\mathrm{re} \pm i\lambda_\mathrm{im})t} \text{ or } \begin{pmatrix} c_1 \\ c_2 \end{pmatrix} \mathrm{Cos}(Kr)\mathrm{e}^{(\lambda_\mathrm{re} \pm i\lambda_\mathrm{im})t} \tag{19.5.10}$$

in which $\begin{pmatrix} c_1 \\ c_2 \end{pmatrix}$ is the eigenvector with the eigenvalue $\lambda = \lambda_{re} \pm i\lambda_{im}$, with its real and imaginary parts as shown. If the real part λ_{re} is positive, the perturbation (19.5.10) will grow. The unstable perturbation contains oscillations in time, due to the factor $e^{i\lambda_{im}t}$ as well as variations in space due to the factor Sin *Kr* or Cos *Kr*. Such a perturbation corresponds to a **propagating wave**.

For matrix (19.5.8), the condition for one of its two real eigenvalues to cross zero can be obtained as follows. First we note that the determinant, Det, of a matrix is the product of the eigenvalues. If the eigenvalues are λ_+ and λ_-, we have

$$\begin{aligned}(\lambda_+\lambda_-) = \text{Det} = (k_2[\text{B}] - k_4 - K^2D_\text{X})\ (-k_3[\text{X}]_\text{s}^2 - K^2D_\text{Y}) \\ + (k_2[\text{B}])(k_3[\text{X}]_\text{s}^2)\end{aligned} \tag{19.5.11}$$

Before the onset of the instability, both eigenvalues are negative and hence Det > 0. Let us assume that when the parameter [B] is varied, λ_+ crosses zero and becomes positive. Then, at the point where $\lambda_+ = 0$, we have Det = 0 and when $\lambda_+ > 0$ we have Det < 0. Thus the condition for the instability may be stated as

$$\text{Det} = (k_2[\text{B}] - k_4 - K^2D_\text{X})(-k_3[\text{X}]_\text{s}^2 - K^2D_\text{Y}) + (k_2[\text{B}])(k_3[\text{X}]_\text{s}^2) < 0 \tag{19.5.12}$$

Using $[\text{X}]_\text{s} = (k_1/k_4)[\text{A}]$ this inequality can be rewritten as

$$[\text{B}] > \frac{1}{k_2}[k_4 + K^2D_\text{X}]\left[1 + \frac{k_3k_1^2[\text{A}]^2}{k_4^2}\frac{1}{K^2D_\text{Y}}\right] \tag{19.5.13}$$

This then is the condition under which a Turing structure will arise in the Brusselator model. As [B] increases, the lowest value $[\text{B}]_\text{c}$ for which (19.5.13) is satisfied will trigger an instability. The value of $[\text{B}]_\text{c}$ can be found by plotting

$$[\text{B}]_\text{c} = \frac{1}{k_2}[k_4 + K^2D_\text{X}]\left[1 + \frac{k_3k_1^2[\text{A}]^2}{k_4^2}\frac{1}{K^2D_\text{Y}}\right] \tag{19.5.14}$$

as a function of K^2. As shown in Figure 19.11, this plot has a minimum. When [B] reaches this minimum value, the corresponding K_min will be the wavenumber of the stationary pattern. The minimum occurs at the following values (Exercise 19.9):

$$K_\text{min}^2 = A\sqrt{\frac{k_3k_1^2}{k_4D_\text{X}D_\text{Y}}} \quad \text{and} \quad [\text{B}]_\text{c} = [\text{B}]_\text{min} = \frac{1}{k_2}\left[\sqrt{k_4} + A\sqrt{\frac{D_\text{X}k_3k_1^2}{D_\text{Y}k_4^2}}\right]^2 \tag{19.5.15}$$

Experimentally, traveling waves have been observed in the Belousov–Zhabotinsky reaction (Figure 19.12) but only recently have the Turing patterns been realized in the laboratory [33].

The examples shown in this chapter are only a small part of the rich variety of behavior encountered in far-from-equilibrium chemical systems. Here our objective is only to show a few examples; an extensive description would form a book in itself! At the end of the chapter there is a list of monographs and conference proceedings that give a detailed descriptions of oscillations, propagating waves, Turing structures, pattern formation on catalytic surfaces, multistability and chaos (both temporal and spatiotemporal). Dissipative structures have also been found in other fields such as hydrodynamics and optics.

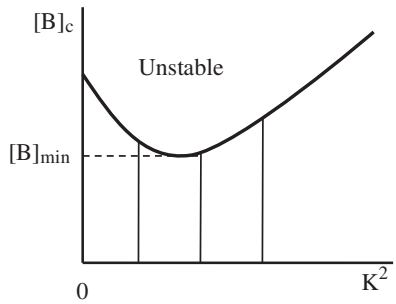

Figure 19.11 *Stability diagram showing the value of [B] and the corresponding value of* K^2 *that will become unstable and grow. The values of* K *that are consistent with the boundary conditions are discrete modes characterized by an integer* m. *As [B] increases, when it is just above* $[B]_{min}$, *the mode* m *that becomes unstable first grows into a spatial structure.*

19.6 Dissipative Structures and Machines

Having studied some examples of dissipative structures, it is interesting to compare them with machines/computers or *designed structures*, for there are some notable and interesting fundamental differences that have been insightfully noted by Robert Rosen [34].

First, we note that most designed structures are based on time-reversible mechanics, classical or quantum; i.e. their mathematical description is based on the reversible dynamical processes. The ideal designed structure

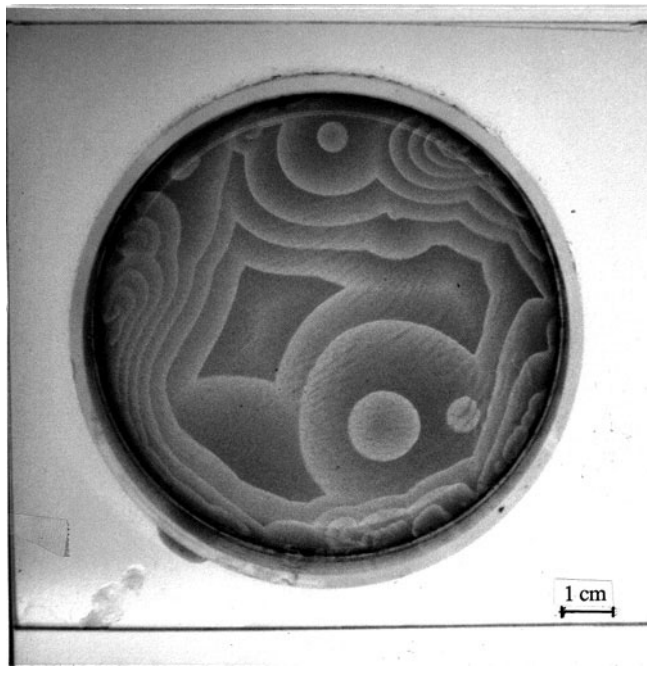

Figure 19.12 *Traveling waves in the Belousov–Zhabotinsky reaction.*

does not include irreversible processes; for its best performance, entropy-generating dissipative processes must be minimized. In stark contrast, the very existence of dissipative structures depends on dissipative processes. Their mathematical description is based on irreversible thermodynamic processes. Their behavior is not time symmetric.

Second, the structure of a designed structure originates from a processes external to the system and so is its function: every designed structure is designed to perform a specific set of functions, as are its components. In computers, 'machine intelligence' is, in fact, 'borrowed intelligence'; the algorithms that enable it to perform its function originate in processes external to the system. Even if a computer can generate an algorithm, it can do so only because it has been supplied with a higher-level algorithm that enables it to do so. In contrast, the structure in dissipative structures originates from processes within. Their behavior, if it could be interpreted as a 'function', is entirely a consequences of self-organization. In a complex dissipative structure, one may associate 'functions' to various subsystems, but those functions are entirely self-generated. If one could associate an 'algorithm' for its behavior, that too originates from within.

Finally, thermodynamic stability of dissipative structure means dissipative processes restore the structure if it is perturbed or 'damaged' – within bounds, of course. This bestows them with the property of 'self-healing'. This is clearly not the case with machines or computers.

From these observations, one may surmise that dissipative structures are more akin to biological organisms than are machines and computers. The machine paradigm is inappropriate as a theory of biological organism. This aspect will be discussed further in the concluding Chapter 21.

19.7 Structural Instability and Biochemical Evolution

We conclude this chapter with a few remarks on another kind of instability often called 'structural instability' and its relevance to biochemical evolution. In the previous sections we have seen instabilities giving rise to organized states. These instabilities arose in a given set of chemical reactions. In nonequilibrium chemical systems, instability may also arise by the introduction of a new chemical species that gives rise to new reactions; these new reactions may destabilize the system and drive it to a new state of organization. In this case the 'structure' of the chemical reaction network is itself subject to changes. Each new species alters the reaction kinetics and this may drastically alter the state of the system; i.e. due to the appearance of a new chemical species the system may become unstable and evolve to a new state.

This type of structural instability can be seen most easily in the evolution of self-replicating molecules with a steady supply of monomers. Let us consider a set of autocatalytic polymers that are capable of self-replication through a template mechanism. In this case, each new polymer is a new autocatalytic species. Let us further assume that this self-replication is subject to random errors or mutations. Each mutation of a self-replicating molecule introduces a new species and new chemical reactions. Thus if we write a set of kinetic equations for such a system, each time a random mutation occurs, the set of equations itself will change. Under a given set of nonequilibrium conditions or 'environment' some (or perhaps most) of the mutations may not produce a polymer whose rate of self-replication is larger than those of others. The appearance of such a new species may cause a small change in the population of various polymers but no significant change will arise. However, some of the mutations might give rise to a polymer with a high rate of self-replication. This would correspond to fluctuation to which the system is unstable. The new polymer may now dominate the system and alter the population significantly. This of course corresponds to Darwinian evolution at the molecular level, the paradigm of the 'survival of the fittest'. Many detailed studies of such structural instabilities and molecular evolution have been conducted [35–38]. These models are beyond the scope of this text but we will note an interesting thermodynamic feature summarized in Figure 19.13. Each new structural instability generally increases the dissipation or the rate of entropy production in the system because it increases the number of

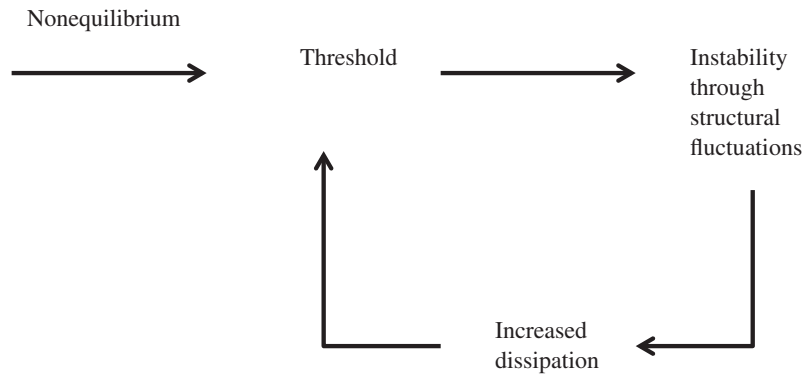

Figure 19.13 *Structural instabilities during molecular evolution give rise to new processes that tend to increase entropy production.*

reactions. This is in contrast to the near-equilibrium situations discussed in Chapter 17 in which the entropy production tends to a minimum. Structural instability may progressively drive far-from-equilibrium systems to higher rates of entropy production and higher states of order. Needless to say, biochemical evolution and the origin of life is a very complex process that we are only beginning to understand. However, now we see instability, fluctuation and evolution to organized states as a general nonequilibrium process whose most spectacular manifestation is the evolution of life.

Appendix 19.1 *Mathematica* Codes

The following codes give the numerical solutions for the kinetic equations for the systems discussed in this chapter. As in Chapter 9, **NDSolve** is used to obtain numerical solutions. The results can be plotted using the **Plot** command. Numerical output can be exported to graphing software using the **Export** command.

CODE A: CHIRAL SYMMETRY BREAKING

```
 (*Code to show chiral symmetry breaking. Kinetic constants are
chosen such that the equilibrium constant,(kf/kr), for direct and
catalyzed reactions are equal*)

k1f=0.5;k1r=0.2;k2f=0.5;k2r=(k1r/k1f)*k2f ;k3f=1.5;k3r=10^-3;
S=1.25;T=S;P=0.5;

R1f:=k1f*S*T;R1r:=k1r*XL[t];
R2f:=k2f*S*T*XL[t];R2r:=k2r*(XL[t])^2;
R3f:=k1f*S*T;R3r:=k1r*XD[t];
R4f:=k2f*S*T*XD[t];R4r:=k2r*(XD[t])^2;
R5f:=k3f*XL[t]*XD[t];R5r:=k3r*P;

(* Initial values of XL and XD are set at steady state values for S=0.5 *)

Soln1=NDSolve[{XL'[t]==R1f-R1r+R2f-R2r-R5f+R5r,
               XD'[t]==R3f-R3r+R4f-R4r-R5f+R5r,
```

```
                XL[0]==0.2502,XD[0]==0.2500},{XL,XD},{t,0,2000},
                MaxSteps->10000]

tmax=100;

Plot[Evaluate[{XL[t],XD[t]}/.Soln1],{t,0,tmax},
     AxesLabel->{"time","[XL]&[XD]"},
     AxesStyle->Directive[Black,14],
     PlotStyle->{{Black,Thick},{Gray,Thick}},PlotRange->All]

{{XL->InterpolatingFunction[{{0.,2000.}},<>],
  XD->InterpolatingFunction[{{0.,2000.}},<>]}}
```

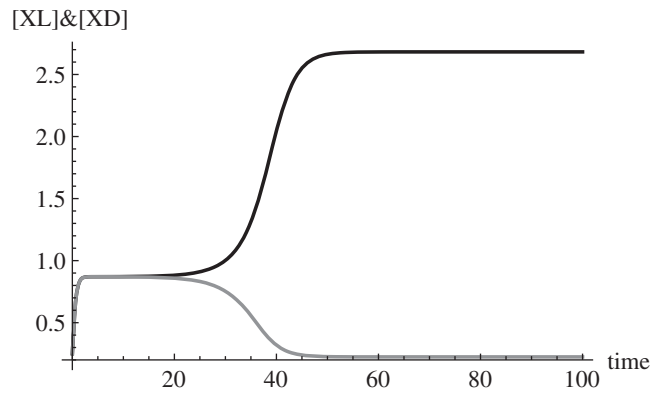

To write output files for spreadsheets, use the **Export** command and the file format List. For more detail see the *Mathematica* help file for the **Export** command. In the command below, the output filename is: data1.txt. This file can be read by most spreadsheets and graphing software.

The command X[t]/.Soln1 specifies that X[*t*] is to be evaluated using Soln1 defined above. TableForm outputs data in a convenient form.

```
Export["data1.txt",Table[{t,{XL[t],XD[t]}/.Soln1},{t,1,50}]//
TableForm, "List"]

data1.txt
```

To obtain a table of *t* versus X(*t*) the following command can be used.

```
Table[{t,{XL[t],XD[t]}/.Soln1},{t,1,5}]//TableForm

1   0.774193  0.773908
2   0.860958  0.860593
3   0.86964   0.869178
4   0.870507  0.869924
5   0.870658  0.869922
```

The rate of entropy production due to each of the reactions in the above scheme can be calculated using the following code. The Plot command plots the total rate of entropy production. The Table command outputs a table of the rates of entropy production for each reaction at the last three time points.

```
RR=8.314;
Sig1:=RR*(R1f-R1r)*Log[R1f/R1r];
Sig2:=RR*(R2f-R2r)*Log[R2f/R2r];
Sig3:=RR*(R3f-R3r)*Log[R3f/R3r];
Sig4:=RR*(R4f-R4r)*Log[R4f/R4r];
Sig5:=RR*(R5f-R5r)*Log[R5f/R5r];
SigTot:=Sig1+Sig2+Sig3+Sig4+Sig5;

Plot[Evaluate[SigTot/.Soln1], {t,10,tmax},
     AxesLabel->{"time","[XL]&[XD]"},
     AxesStyle->Directive[Black,14],
     PlotStyle->{Black,Thick},PlotRange->All]

Table[TableForm[{Evaluate[{t,SigTot,Sig1,Sig2,Sig3,Sig4,Sig5}
/.Soln1]}], {t,tmax-2,tmax}]
```

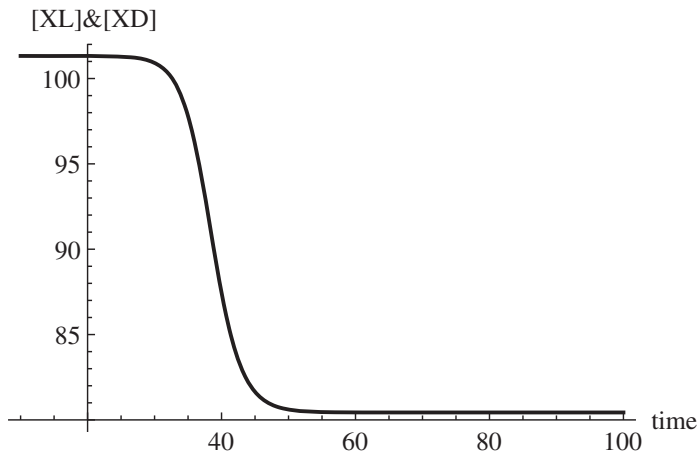

98	99	100
80.4352	80.4352	80.4352
0.765395	0.765395	0.765395
2.05282	2.05282	2.05282
17.4965	17.4965	17.4965
3.92293	3.92293	3.92293
56.1976	56.1976	56.1976

CODE B: THE BRUSSELATOR

The following is the code for the Brusselator. Since no reverse reactions are involved, we shall not use the subscripts f and r for the reaction rates and rate constants.

```
(* Chemical Kinetics:  The Brusselator *)

k1=1.0; k2=1.0; k3=1.0; k4=1.0; A=1.0; B=3.0;
R1:=k1*A; R2:=k2*B*X[t]; R3:=k3*(X[t]^2)*Y[t];
R4:=k4*X[t];


Soln2=NDSolve[{X'[t]== R1-R2+R3-R4,
               Y'[t]== R2-R3,
               X[0]==1.0,Y[0]==1.0},
               {X,Y},{t,0,20},
               MaxSteps->500]

 {{X->InterpolatingFunction[{{0.,20.}},<>],
   Y->InterpolatingFunction[{{0.,20.}},<>]}}

Plot[Evaluate[{X[t]}/.Soln2],{t,0,20},PlotRange->{0,4},
     PlotStyle->{Black,Thick},
     AxesLabel->{"time"},
     AxesStyle->Directive[Black,14]]
```

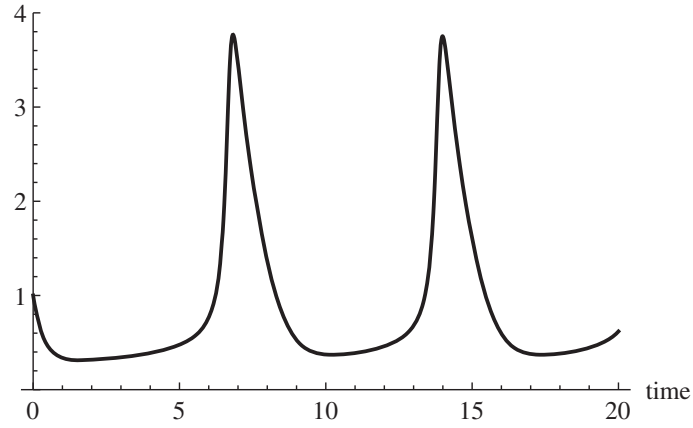


```
Plot[Evaluate[{X[t],Y[t]}/.Soln2],{t,0,20},
     PlotStyle->{{Black, Thick},{Gray,Thick}},
     AxesLabel->{"time"},
     AxesStyle->Directive[Black, 14]]
```

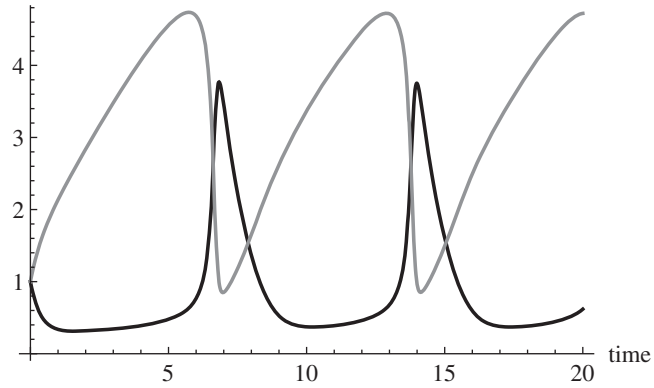


```
Table[{t,Evaluate[{X[t],Y[t]}/.Soln2]},{t,0,10,1}]
//TableForm
```

```
0  1. 1.
1  0.336806  2.13473
2  0.316947  2.83679
3  0.344197  3.48043
4  0.389963  4.0695
5  0.476012  4.556
6  0.766335  4.6843
7  3.45363   0.851828
8  1.36836   1.6496
9  0.526035  2.63
10 0.373265  3.36134
```

CODE C: THE BELUSOV–ZHABOTINSKY REACTION

The following is the FKN model of the Belousov–Zhabotinsky reaction. Since no reverse reactions are involved, we shall not use the subscripts f and r for the reaction rates and rate constants.

```
 (* The Belousov-Zhabotinsky Reaction/FKN Model *)

(* X=HBrO2      Y=Br-      Z=Ce4+     B=Org      A=BrO3- *)

k1=1.28; k2=8.0; k3=8.0*10^5; k4=2*10^3; k5=1.0;
A=0.06; B=0.02;f=1.5;

R1:=k1*A*Y[t];  R2:=k2*A*X[t];  R3:=k3*X[t]*Y[t];
R4:=k4*X[t]^2;  R5:=k5*B*Z[t];

Soln3=NDSolve[{X'[t]== R1+R2-R3-2*R4,
               Y'[t]== -R1-R3+(f/2)*R5,
               Z'[t]== 2*R2-R5,
```

```
            X[0]==2*10^-7,Y[0]==0.00002,Z[0]==0.0001},
            {X,Y,Z},{t,0,1000}, MaxSteps->2000]

{{X->InterpolatingFunction[{{0.,1000.}},<>],
  Y->InterpolatingFunction[{{0.,1000.}},<>],
  Z->InterpolatingFunction[{{0.,1000.}},<>]}}

Plot[Evaluate[{Z[t],10*X[t]}/.Soln3],{t,0,900},
     PlotRange->{0.0,1.5*10^-3},
     PlotStyle->{{Black, Thick},{Gray,Thick}},
     AxesStyle->Directive[Black, 14]]
```

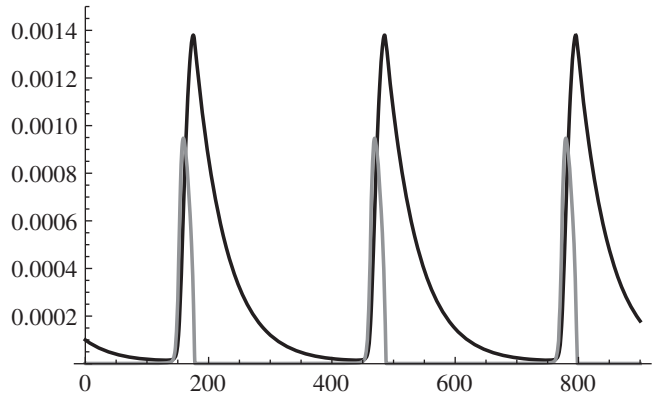

References

1. Prigogine, I., *From Being to Becoming*. 1980, W.H. Freeman: San Francisco, CA.
2. Prigogine, I., Stengers, I., *Order Out of Chaos*. 1984, Bantam: New York.
3. Prigogine, I., *Introduction to Thermodynamics of Irreversible Processes*. 1967, John Wiley & Sons, Inc.: New York.
4. Kondepudi, D.K., Nelson, G.W., Chiral-symmetry-breaking states and their sensitivity in nonequilibrium chemical systems. *Physica A*, **125** (1984), 465–496.
5. Hegstrom, R., Kondepudi, D.K., The handedness of the Universe. *Sci. Am.*, January 1990, 108–115.
6. Mason, S.F., Tranter, G.E., The parity-violating energy difference between enantiomeric molecules. *Chem. Phys. Lett.*, **94** (1983), 34–37.
7. Hegstrom, R.A., Rein, D.W., Sandars, P.G.H., Calculation of the parity nonconserving energy difference between mirror-image molecules. *J. Chem. Phys.*, **73** (1980), 2329–2341.
8. Frank, F.C., On spontaneous asymmetric synthesis. *Biochem. Biophys. Acta*, **11** (1953), 459–463.
9. Kondepudi, D.K., Kaufman, R., Singh, N., Chiral symmetry breaking in sodium chlorate crystallization. *Science*, **250** (1990), 975–976; Kondepudi, D.K., *et al.*, Kinetics of chiral symmetry breaking in crystallization. *J. Am. Chem. Soc.*, **115** (1993), 10211–10216; Viedma, C., Chiral symmetry breaking during crystallization: complete chiral purity induced by nonlinear autocatalysis and recycling. *Phys. Rev. Lett.*, **94** (2005), 065504–065506.
10. Soai, K., Shibata, T., Sato, I., Enantioselective automultiplication of chiral molecules by asymmetric autocatalysis. *Accounts of Chemical Research*, **33** (2000), 382–390; Blackmond, D., Kinetic aspects of nonlinear effects in asymmetric catalysis. *Account of Chemical Research*, **33** (2000), 402–411.
11. Bonner, W.A., The origin and amplification of biomolecular chirality. *Origins of Life and Evol. Biosphere*, **21** (1991), 59–111.

12. Bonner, W.A., Terrestrial and extraterrestrial origin of molecular homochirality. *Origins of Life and Evol. Biosphere*, **21** (1992), 407–420.
13. Bouchiat, M.-A., Pottier, L., Optical experiments and weak interactions. *Science*, **234** (1986), 1203–1210.
14. Mason, S.F., Tranter, G.E., The electroweak origin of biomolecular handedness. *Proc. R. Soc. London*, **A397** (1985), 45–65.
15. Kondepudi, D.K., Asakura, K., Chiral autocatalysis, spontaneous symmetry breaking, and stochastic behavior. *Accounts of Chemical Research*, **34** (2001), 446–454.
16. Kondepudi, D.K., Nelson, G.W., Weak neural currents and the origin of biomolecular chirality. *Nature*, **314** (1985), 438–441.
17. Hegstrom, R., Weak neural current and β radiolysis effects on the origin of biomolecular chirality. *Nature*, **315** (1985), 749–751.
18. Kondepudi, D.K., Selection of molecular chirality by extremely weak chiral interactions under far-from-equilibrium conditions. *BioSystems*, **20** (1987), 75–83.
19. Cline, D.B. (ed.), *Physical Origin of Homochirality in Life*. 1996, American Institute of Physics: New York.
20. Winfree, A.T., The prehistory of the Belousov–Zhabotinsky oscillator. *J. Chem. Ed.*, **61** (1984), 661–663.
21. Prigogine, I., Lefever, R., Symmetry breaking instabilities in dissipative systems. II. *J. Chem. Phys.*, **48** (1968), 1695–1700.
22. Zhabotinsky, A.M., Periodic liquid phase reactions. *Proc. Ac. Sci. USSR*, **157** (1964), 392–395; Zaikin, A.N., Zhabotinsky, A.M., Concentration wave propagation in two-dimensional liquid-phase self-oscillating system. *Nature* (1970), **225**, 535–537.
23. Field, R.J., Körös, E., Noyes, R.M., Oscillations in chemical systems. II. Thorough analysis of temporal oscillation in the bromite–cerium–malonic acid system. *J. Am. Chem. Soc.*, **94** (1972), 8649–8664.
24. Field, R.J., Burger, M. (eds), *Oscillations and Traveling Waves in Chemical Systems*. 1985, John Wiley & Sons, Inc.: New York.
25. Gray, P., Scott, K.S., *Chemical Oscillations and Instabilities*, 1990, Clarendon Press: Oxford.
26. Epstein, I.R., Showalter, K., Nonlinear chemical dynamics: oscillations, patterns, and chaos. *J. Phys. Chem.*, **100** (1996), 13132–13143.
27. Epstein, I.R., Orban, M., in *Oscillations and Traveling Waves in Chemical Systems*, R.J.F. Fiel and M. Burger (eds). 1985, John Wiley & Sons, Inc.: New York.
28. Epstein, I., Kustin, K., De Kepper, P., Orbán, M., Oscillating chemical reactions. *Sci. Am.*, March 1983, 96–108.
29. Epstein, I.R., The role of flow systems in far-from-equilbrium dynamics. *J. Chem. Ed.*, **69** (1989), 191.
30. Boissonade, J., Dekepper, P., Transitions from biostability to limit cycle oscillations. Theoretical analysis and experimental evidence in an open chemical system. *J. Phys. Chem.*, **84** (1980), 501–506.
31. Goldbeter, A., *Biochemical Oscillations and Cellular Rhythms: The Molecular Bases of Periodic and Chaotic Behaviour*. 1996, Cambridge University Press: Cambridge.
32. Turing, A., The chemical basis of morphogenesis. *Phil. Trans. R. Soc. London*, **B237** (1952), 37–72.
33. Kapral, R., Showalter, K. (eds), *Chemical Waves and Patterns*. 1994, Kluwer: New York.
34. Rosen, R., *Essays on Life Itself*. 2000, Columbia University Press, New York.
35. Prigogine, I., Nicolis, G., Babloyantz, A., Thermodynamics in evolution. *Physics Today*, **25** (1972), No. 11, 23; No. 12, 38.
36. Eigen, M., Schuster, P., *The Hypercycle – A Principle of Natural Self-organization*. 1979, Springer: Heidelberg.
37. Nicolis, G., Prigogine, I., *Self-organization in Nonequilibrium Systems*. 1977, John Wiley & Sons, Inc.: New York.
38. Küppers, B.-O., *Molecular Theory of Evolution*. 1983, Springer Verlag: Berlin.

Further Reading

Baras, F., Walgraef, D. (eds), Nonequilibrium chemical dynamics: from experiment to microscopic simulation. *Physica A*, **188** (1992), No. 1–3; special issue.

Ciba Foundation Symposium 162, *Biological Asymmetry and Handedness*. 1991, John Wiley & Sons, Ltd: London, Chichester.

Epstein, I., Pojman, J., *An Introduction to Nonlinear Chemical Dynamics: Oscillations, Waves, Patterns and Chaos*. 1998, Oxford University Press: New York.

Field, R.J., Burger, M. (eds), *Oscillations and Traveling Waves in Chemical Systems.* 1985, John Wiley & Sons, Inc.: New York.

Goldbeter, A., *Biochemical Oscillations and Cellular Rhythms: The Molecular Bases of Periodic and Chaotic Behaviour*. 1996, Cambridge University Press, Cambridge.

Gray, P., Scott, K.S., *Chemical Oscillations and Instabilities.* 1990, Clarendon Press: Oxford.

Kapral, R., Showalter, K. (eds), *Chemical Waves and Patterns.* 1994, Kluwer: New York.

Manneville, P., *Dissipative Structures and Weak Turbulence.* 1990, Academic Press: San Diego, CA.

Nicolis, G., Prigogine, I., *Self-Organization in Nonequilibrium Systems.* 1977, John Wiley & Sons, Inc.: New York.

State-of-the-Art Symposium: Self-Organization in Chemistry. *J. Chem. Ed.*, **66** (1989), No. 3; articles by several authors.

Vidal, C., Pacault, A. (eds), *Non-Linear Phenomenon in Chemical Dynamics.* 1981, Springer Verlag: Berlin.

Exercises

19.1 Analyze the stability of solutions $\alpha = 0$ and $\alpha = \pm\sqrt{\lambda}$ for Equation (19.2.1) and show explicitly that when $\lambda > 0$ the solution $\alpha = 0$ becomes unstable whereas the solutions $\alpha = \pm\sqrt{\lambda}$ are stable.

19.2 Write a *Mathematica* or *Maple* code to obtain the solutions of the equations in Exercise 19.1. Plot these solutions as a function of time for various initial conditions and show explicitly that the solutions evolve to stable stationary states.

19.3 For the reaction scheme (19.3.1) to (19.3.5), using the principle of detailed balance, verify that the concentrations of X_L and X_D will be equal at equilibrium.

19.4 Using the variables α, β and λ defined in (19.3.8), show that the kinetic equations (19.3.6) and (19.3.7) can be written in the forms of (19.3.9) and (19.3.10).

19.5 Show that Equation (19.4.7) are the stationary states of the kinetic equations of the Brusselator equations (19.4.5) and (19.4.6).

19.6 **(a)** Write the kinetic equations for [X] and [Y], assuming that [A] and [B] are fixed, for the following scheme (called the Lotka–Volterra model):

$$\mathrm{A} + \mathrm{X} \rightarrow 2\mathrm{X}, \qquad \mathrm{X} + \mathrm{Y} \rightarrow 2\mathrm{Y}, \qquad \mathrm{Y} \rightarrow \mathrm{B}$$

(b) Obtain its steady states and analyze their stability as a function of the parameters [A] and [B].

19.7 **(a)** Using the dimensionless variables defined by

$$x = \frac{[\mathrm{X}]}{X_0}, \qquad y = \frac{[\mathrm{X}]}{Y_0}, \qquad z = \frac{[Z]}{Z_0} \text{ and } \tau = \frac{t}{T_0}$$

in which

$$X_0 = \frac{k_2[\mathrm{A}]}{2k_4}, \quad Y_0 = \frac{k_2[\mathrm{A}]}{k_3}, \quad Z_0 = \frac{(k_2[\mathrm{A}])^2}{k_4 k_5[\mathrm{B}]}, \quad T_0 = \frac{1}{k_5[\mathrm{B}]}$$

show that the kinetic equations (19.4.16) to (19.4.18) can be written as

$$\varepsilon \frac{\mathrm{d}x}{\mathrm{d}\tau} = qy - xy + x(1 - x)$$

$$\varepsilon' \frac{\mathrm{d}x}{\mathrm{d}\tau} = -qy - xy + fz$$

$$\frac{\mathrm{d}z}{\mathrm{d}\tau} = x - z$$

in which

$$\varepsilon = \frac{k_5[\mathrm{B}]}{k_2[\mathrm{A}]}, \quad \varepsilon' = \frac{2k_5k_4[\mathrm{B}]}{k_3k_2[\mathrm{A}]} \text{ and } q = \frac{2k_1k_4}{k_3k_2}$$

(See Tyson, J.J., Scaling and reducing the Field–Körös–Noyes mechanism of the Belousov–Zhabotinsky reaction, *J. Phys. Chem.*, **86** (1982), 3006–3012.)

(b) Find the stationary states of this set of equations.

19.8 Using *Mathematica* Code C in Appendix 19.1, obtain the range of values for the parameter f in which oscillations occur. Also plot the relation between the period of oscillations and the value of f.

19.9 Show that the minimum of Equation (19.5.14) occurs at the values given by Equation (19.5.15).